PNAS RESEARCH ARTICLE | PSYCHOLOGICAL AND COGNITIVE SCIENCES OPEN ACCESS

Automaticity speeds the retrieval of instances from the human hippocampus

Yuanyuan Zhang[a,b,c,1], Junxi Chen[d,1], Geoffrey F. Woodman[e,f], Rongqi Lin[a,b,c], Fuyong Chen[g,2], Xuchu Weng[b,2], Ole Jensen[h], Jan Theeuwes[c], and Benchi Wang[b,2]

Affiliations are included on p. 9.

Edited by Richard Shiffrin, Indiana University, Bloomington, IN; received July 24, 2025; accepted September 18, 2025

Automatic processing allows humans to perform tasks with minimal effort following learning. Although theories of automaticity propose that learning should result in faster processing, studies have universally found that learning reduces the amplitude of neural activity, not that it speeds neural activity. Here, we show that with intracranial activity recorded from the hippocampus of twenty-two humans, we could decode the target the participant was about to report faster across learning. Theta oscillations in the hippocampus afforded faster decoding of the to-be-reported target as learning progressed, unlike in prefrontal and temporal regions of the cortex. Furthermore, hippocampal ripples (70 to 180 Hz bursts) appear to support memory retrieval after learning established automaticity. Our findings demonstrate that the hippocampus plays a key role in speeding memory retrieval of previous learning episodes as humans gain expertise, supporting a critical but untested prediction of learning theories.

automaticity | hippocampus | theta oscillation | intracranial EEG

Significance

Do you ever find yourself driving without remembering how you got through the last set of intersections? If so, you experience the benefit of automaticity, that is performing a task without much conscious thought. The present study shows that our ability to drive automatically comes from quickly retrieving memories of what you did when driving through those intersections previously. By measuring intracranially electrical activity from the hippocampus, we could decode what information this memory structure of the brain was retrieving from memory. In addition, this happens faster and faster with learning, supporting crucial predictions of models that explain how we achieve automatic levels of performance. These findings show how we acquire skills and how our memory works in daily life.

To investigate the neural dynamics of the hippocampus during the acquisition of automaticity, we collected and analyzed intracranial electroencephalography (iEEG) data from neurosurgical patients engaged in a simple task that involved extensive practice (1–3). Our analysis included signals from the hippocampus, prefrontal cortex, and middle-temporal gyrus to compare hippocampal responses with other cortical brain structures. Employing multivariate pattern analysis, we extracted representation-specific information and identified the moments and locations where the brain represented the information that the participant was about to report. Our analysis focused on theta band oscillations (4 to 8 Hz), which have been shown to play a critical role in learning and memory (4–10). Additionally, we analyzed ripple activity, commonly identified as high-frequency activity which is known to correlate with memory retrieval (11–17).

Experiment 1

Eighteen participants were instructed to memorize the random order of two fixed orientations presented in succession on each trial of the experiment. After one left and one right titled grating stimulus were shown, participants were asked to report either the first or the second orientation as directed by a cue. They indicated the orientation by rotating a grating with a mouse (see Fig. 1*A* and *Methods* for details). The two orientations were fixed across trials (e.g., 45 and 135°) to make the task simple and minimize the number of stimuli that the patients needed to learn during the task, allowing for the formation of automaticity through repeated visual-motor experience (1–3). The participants' performance improved over trials. Specifically, participants exhibited fewer errors and faster response times in the late stage (last 90 trials; mean errors = 13.2°, mean RT = 3,377 ms) compared to early stage (first 90 trials; mean errors = 16.2°, mean RT = 4,280 ms), $t(17) = 2.14$, $P = 0.048$, Cohen's d = 0.5 and $t(17) = 2.76$, $P = 0.013$, Cohen's d = 0.65, respectively.

We observed a reduction in power across multiple frequencies (ranging from 1 to 85 Hz) following the presentation of memory items and the cue in the middle-temporal gyrus and prefrontal cortex. Importantly, in the hippocampus there was not a reduction in lower frequencies (<14 Hz). We did not observe significant differences in power for these brain areas when comparing the early with late stage. Detailed results can be found in Supplementary Information (*SI Appendix*, Fig. S1).

Following cue presentation (Fig. 1*A*), we used participants' brain activity to decode the to-be-reported orientation from different brain regions over time. This was accomplished by employing a support vector machine (SVM) for multivariate classification

Author contributions: B.W. designed the experiment; Y.Z., J.C., R.L., and F.C. collected the data; Y.Z., R.L., O.J., and B.W. analyzed the data; and Y.Z., J.C., G.F.W., R.L., F.C., X.W., O.J., J.T., and B.W. wrote the paper together and approved the final version of the manuscript for submission.

The authors declare no competing interest.

This article is a PNAS Direct Submission.

Copyright © 2025 the Author(s). Published by PNAS. This open access article is distributed under Creative Commons Attribution-NonCommercial-NoDerivatives License 4.0 (CC BY-NC-ND).

[1]Y.Z. and J.C. contributed equally to this work.

[2]To whom correspondence may be addressed. Email: chenfy@hku-szh.org, wengxc@psych.ac.cn, or wangbenchi.swift@gmail.com.

This article contains supporting information online at https://www.pnas.org/lookup/suppl/doi:10.1073/pnas.2518523122/-/DCSupplemental.

Published October 30, 2025.

Downloaded from https://www.pnas.org by SOUTHERN MEDICAL UNIVERSITY on February 26, 2026 from IP address 58.249.1.69.

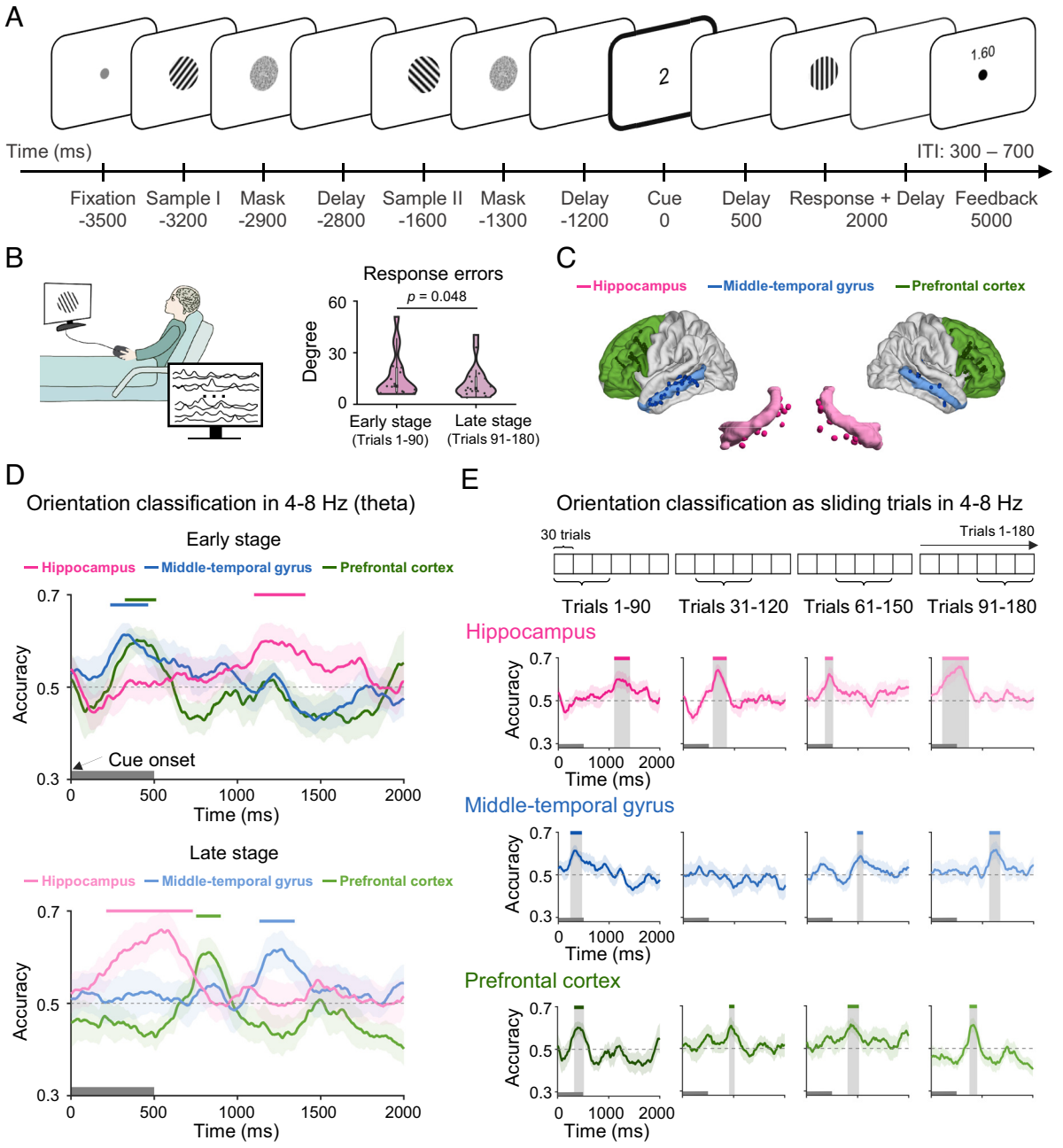


Fig. 1. The procedure and results in Experiment 1. (*A*) Across all trials, participants were instructed to memorize two fixed orientations of gratings presented sequentially. They had to indicate the precise orientation of the cued target by rotating the probe grating with a mouse. The display presenting the cue is highlighted by a bold border. The onset of the cue is set as time 0 ms. (*B*) Intracranial EEG data were recorded while participants performed the simple task with increased efficiency across trials. The *Right* panel shows the mean response errors, with individual response errors represented by solid dots. (*C*) The locations of the recorded contacts in the hippocampus, middle-temporal gyrus, and prefrontal cortex. Solid dots indicate their respective locations. (*D*) Following the presentation of the cue, beginning at 0 ms, we employed a support vector machine (SVM; see *Methods* for details) classifier to decode cued orientation over time from oscillations in the theta band (4 to 8 Hz). Decoding accuracies for different brain regions in two stages (*Top*: early stage including the first 90 trials, *Bottom*: late stage including the last 90 trials) are presented. (*E*) Decoding accuracies are presented after grouping every 90 trials in steps of 30 trials into four blocks across different brain regions. Colored shaded areas around the lines represent ±1 SEM across all participants, and the horizontal bars indicate significant clusters following a cluster-based permutation test ($P < 0.05$). The gray segments on the X-axis denote the presentation of the cue.

(see *Methods* for details) to decode the orientation using theta band activity (4 to 8 Hz) distributed across electrode contacts within a set of brain areas: the hippocampus, middle-temporal gyrus, and prefrontal cortex (Fig. 1*D*). In step one of our analyses, the SVM decoding showed that cued orientation was initially represented in the middle-temporal gyrus (236 to 464 ms) and prefrontal cortex (324 to 512 ms), before being decoded from the hippocampus (1,100 to 1,408 ms; cluster-based permutation tests; $P < 0.05$). This shows that during the initial learning trials in the early stage, the to-be-reported representation is present in cortical structures associated with working memory functions (18–20), prior to being decodable within the hippocampal electrodes.

As expected, based on prior learning studies (21, 22), we saw a significant increase in accuracy from the early to late stage as participants learned the task (Fig. 1*B*). Instance theories predict that as instances accumulate in long-term memory, retrieval becomes progressively faster due to simple statistical sampling encapsulated in the logic of race models (23). Larger samples of runners in a race will have faster finishing times assuming similar

Downloaded from https://www.pnas.org by SOUTHERN MEDICAL UNIVERSITY on February 26, 2026 from IP address 58.249.1.69.

means and variance across runners (1, 24, 25). Competing accounts of automaticity make similar predictions about but propose that the strength of the task-related memories increases across learning resulting in faster memory retrieval (26). In the context of our task, this means that we should observe faster memory retrieval of the correct orientation following the cue that specifies which of the two orientations to report on that trial. Our results aligned with this prediction, revealing significantly faster decoding of the to-be-reported orientation within the hippocampus as the number of trials progressed. Specifically, we could decode the orientation in the hippocampus (212 to 732 ms), followed by the prefrontal cortex (752 to 900 ms), and subsequently the middle-temporal gyrus (1,132 to 1,344 ms; cluster-based permutation tests; $P < 0.05$) in the late stage of the experiment. These findings indicate increasingly rapid hippocampal decoding as participants became more proficient at this simple orientation reporting task, aligning with the predictions of instance theories of automaticity, which make specific predictions about the timing of retrieval as learning advances.

To statistically confirm this conclusion, we selected the peak latency within significant decoding clusters for each participant and entered these values into a two-way ANOVA with factors of learning stage (early vs. late) and brain region (hippocampus, middle-temporal gyrus, and prefrontal cortex). The analysis revealed significant main effects for both learning stage, $F(1,8) = 22.45$, $P = 0.001$, $\eta_p^2 = 0.74$ and brain region, $F(2,16) = 37.91$, $P < 0.001$, $\eta_p^2 = 0.83$, as well as a significant interaction, $F(2,16) = 332.63$, $P < 0.001$, $\eta_p^2 = 0.98$. This interaction underscores the dynamic temporal shift in the hippocampus's role during the task, highlighting its increasing importance in memory retrieval as learning progresses.

How finely grained can we see the effects of learning speeding retrieval in the hippocampus? To observe the temporal dynamics of learning with higher temporal fidelity, we grouped trials in blocks of 90, and shifted them by 30 trials (1 to 90; 31 to 120; 61 to 150; 91 to 180), and then conducted decoding analyses. As illustrated in Fig. 1*E*, the results showed that across practice we could decode the to-be-reported orientation from the hippocampus as progressively earlier timepoints. Specifically, the cued orientation was significantly decodable from the hippocampus during the interval from 1,100 to 1,408 ms post–cue onset for block one, the interval from 576 to 848 ms post–cue onset for block two, the interval from 348 to 508 ms post–cue onset for block three, and the interval from 212 to 732 ms post–cue onset for block four (cluster-based permutation tests, $P < 0.05$).

For the neocortex (middle-temporal gyrus and prefrontal cortex), a reversed pattern was observed. Orientation represented in the middle-temporal gyrus was decoded during the interval from 236 to 464 ms post–cue onset for block one, the interval from 980 to 1,100 ms post–cue onset for block three, and the interval from 1,132 to 1,344 ms post–cue onset for block four (cluster-based permutation tests, $P < 0.05$). Orientation was decoded in the prefrontal cortex in the interval from 324 to 512 ms post–cue onset for block one, the interval from 912 to 1,016 ms post–cue onset for block two, the interval from 804 to 1,024 ms post–cue onset for block three, and the interval from 752 to 900 ms post–cue onset for block four (cluster-based permutation tests, $P < 0.05$). Notably, instead of 90 trials per block, these results pattern held when grouping trials into blocks of 60 with no overlapping trials across blocks.

Previous functional MRI studies of learning have shown reduced activity in these structures across learning (27, 28), but lacked the methods to determine whether the latency was changing. Here, we see that decoding reveals that the neural activity did change its latency, but in a direction that is opposite of the speed up of response time with learning. Overall, the present findings are consistent with the predictions laid out by the computational model of instance theory which proposes that memory representations compete to retrieve the appropriate stimulus–response mapping given the sequence of stimuli on that trial (1, 24). This theory says that long-term memory retrieval should speed up as observers give up on using representations in working memory to perform the task, and we observed faster decoding in long-term memory structures (i.e., the hippocampus), but slower decoding in human brain areas linked to working memory (such as prefrontal cortex).

Hippocampal ripples are high frequency oscillations first identified in rodents (16, 29), but also observed in humans (11, 13, 17). These ripples appear to be related to the retrieval of memories (12, 14, 15), with iEEG recordings in humans showing that ripples predict successful recall (12, 14, 15). This provides us with an additional test of the predictions of theories of automaticity. Specifically, we expect to observe an increase in sharp-wave ripples in the hippocampus across learning, particularly during the period of the trial in which participants need to retrieve the task-appropriate response given the stimulus sequence on that trial.

We identified ripple activity from the raw iEEG signals, which were bandpass filtered in the 70 to 180 Hz range (12) across all contacts for each participant (Fig. 2*A*; for details, see *Methods*). Subsequently, we calculated ripple rates, defined as the frequency of ripples per second, for both the immediate and delayed retrieval periods separately. As shown in Fig. 1*D*, for each brain region, the orientation representation could be decoded at different times for each learning stage in each brain region. Accordingly, we defined the early significant decoding cluster as the immediate retrieval period and the late significant decoding cluster as the delayed retrieval period, separately for each brain region. This definition is supported by prior research showing that the emergence of functional ripples coincides with above-chance decoding (12, 30, 31). These findings guided our selection of specific time windows for analyzing ripple rates, aligning them with significant decoding clusters.

We next conducted a repeated-measures ANOVA with factors (learning stage: early vs. late; retrieval period: immediate vs. delayed) on ripple rates for different brain regions separately (Fig. 2*A*). There were no significant interactions for the hippocampus, $F(1,14) = 0.05$, $P = 0.825$, $\eta_p^2 < 0.01$, prefrontal cortex, $F(1,10) = 0.84$, $P = 0.381$, $\eta_{p_2}^2 = 0.08$, and middle-temporal gyrus, $F(1,14) = 0.41$, $P = 0.534$, $\eta_p^2 = 0.03$); nor main effects of learning stage for the hippocampus, $F(1,14) = 3.75$, $P = 0.073$, $\eta_p^2 = 0.21$, prefrontal cortex, $F(1,10) = 0.83$, $P = 0.385$, $\eta_p^2 = 0.08$, and middle-temporal gyrus, $F(1,14) = 1.39$, $P = 0.259$, $\eta_p^2 = 0.09$. Yet, there was a significant main effect of retrieval period for the hippocampus, $F(1,14) = 6.95$, $P = 0.02$, $\eta_p^2 = 0.33$, and prefrontal cortex, $F(1,10) = 10.69$, $P = 0.008$, $\eta_p^2 = 0.52$, but not for the middle-temporal gyrus, $F(1,14) = 0.54$, $P = 0.474$, $\eta_p^2 = 0.04$. In general, ripple rates in the hippocampus increased from the delayed retrieval period to the immediate retrieval period, consistent with the instance theory predictions that more instances of task practice will result in faster retrieval of the appropriate representations from long-term memory (Fig. 2*A*).

Parallel to the decoding analyses presented previously, we next determined how granularly we could see the increase in ripple rates across learning. To examine this, we divided trials into six subsections, each containing 30 trials, and conducted a repeated-measures ANOVA with subsection as a factor on ripple rates during the immediate retrieval period. The results revealed a significant effect for the hippocampus, $F(1,5) = 2.38$, $P = 0.048$, $\eta_p^2 = 0.15$ (Fig. 2*B*); but not for the prefrontal cortex $F(1,5) = 0.55$, $P = 0.735$, $\eta_p^2 = 0.05$,

Downloaded from https://www.pnas.org by SOUTHERN MEDICAL UNIVERSITY on February 26, 2026 from IP address 58.249.1.69.

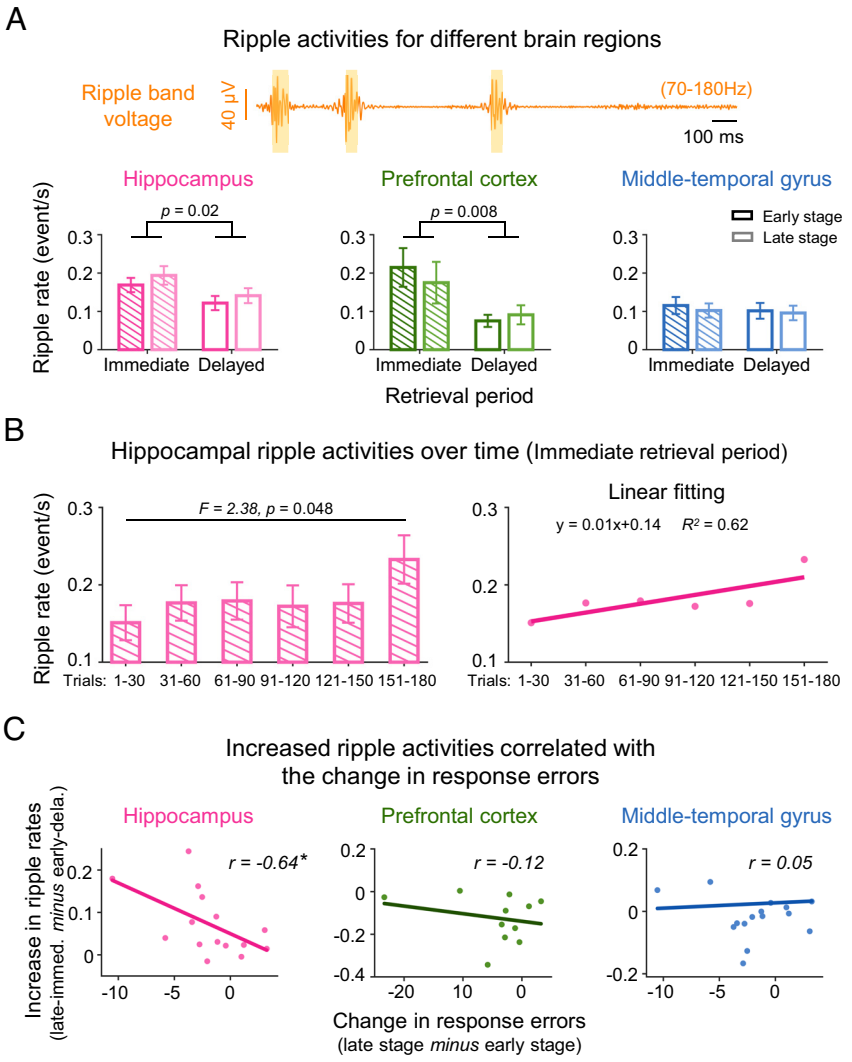


Fig. 2. Ripple activity in Experiment 1. (*A*) *Top* panel: Ripple-band filtered voltage (70 to 180 Hz). Yellow shaded regions indicate representative ripples occurring concurrently. *Bottom* panel: Ripple rates (ripple activity per second) were calculated within the immediate and delayed retrieval period across two learning stages in the corresponding brain regions. The immediate and delayed retrieval periods were defined for different brain regions separately according to their decoding results associated with the respective stages. For example, in the hippocampus, we used the significant decoding cluster observed in the late stage as the immediate retrieval period, while the cluster observed in the early stage was defined as the delayed retrieval period. Error bars indicate ±1 SEM. (*B*) Hippocampal ripple activity changed over time within the immediate retrieval period, following a linear model (R^2 = 0.62; with a positive slope larger than zero, P = 0.033, one-tailed). (*C*) The correlation between the change in behavioral response errors and the increase in ripple rates (from encoding to retrieval) in corresponding brain regions. This analysis revealed a negative correlation for the hippocampus, but not for the prefrontal cortex and middle-temporal gyrus. Colored solid dots represent individual data.

and middle-temporal gyrus, $F(1,5) = 1.2$, $P = 0.317$, $\eta_p^2 = 0.08$ (*SI Appendix*, Fig. S3). Additionally, the change in ripple rate fit a linear model ($R^2 = 0.62$), with a positive slope larger than zero ($P = 0.033$, one-tailed). That is, as the number of trials progressed, the ripple rate during the immediate retrieval period increased from early to late stage of learning the task, confirming a shift over time in the role of the hippocampus to speed memory retrieval after established automaticity. The linear increase in ripple rates in the hippocampus was driven by a sudden increase in the last bin (trials: 151 to 180), indicating a stable retrieval function for the hippocampus during this period. Overall, ripple rates in the hippocampus increased progressively as participants became more automatic at performing the task.

The previous analysis showed that ripple rates increase from the early to late stage of learning the task. However, these neural metrics of retrieval may also correlate with differences in task performance across participants. To investigate this, we calculated the Spearman correlation over participants between the reduction in response errors (late stage minus early stage) and the increase in ripple rates (immediate retrieval period in the late stage minus delayed retrieval period in the early stage). This analysis revealed a negative correlation for the hippocampus, $r = -0.64$, $P = 0.012$ (Fig. 2*C*), but not for the prefrontal cortex, $r = -0.12$, $P = 0.734$, and the middle-temporal gyrus, $r = 0.05$, $P = 0.873$.

In Experiment 1, using machine learning to decode the presence of useful neural information from intracranial recordings of the human brain, we successfully decoded the to-be-reported orientation given the response cue from the theta power across electrode contacts in the hippocampus, middle-temporal gyrus, and prefrontal cortex. In the early stage of learning (i.e., the first 90 trials), the to-be-reported orientation was initially decoded from the neocortex (middle-temporal gyrus and prefrontal cortex) before being decoded from the hippocampus. This pattern was reversed for the late stage of learning (i.e., the last 90 trials), where the orientation was initially decoded from the hippocampus before being decoded from the neocortex. We also observed hippocampal ripple rates showed a linear increase over time during the immediate retrieval period from the early to late learning stage. This

Downloaded from https://www.pnas.org by SOUTHERN MEDICAL UNIVERSITY on February 26, 2026 from IP address 58.249.1.69.

provides converging evidence supporting the predictions of instance theories of learning that propose that skill acquisition is due to faster and more potent memory retrieval across trials.

Experiment 2

Although a temporal shift in hippocampal decoding was observed from the early to late stages in Experiment 1, we also found activity in the prefrontal cortex and middle-temporal gyrus—regions not typically assumed to be involved in automaticity (26, 32, 33). This raises the possibility that the limited training in Experiment 1 (180 trials) may have been insufficient for participants to achieve true automaticity. To address this, Experiment 2 involved four new participants who had contacts recorded from the hippocampus and prefrontal cortex. It implemented an extensive training process involving 1,620 trials across nine training sessions, followed by a test session over three consecutive days. Each training session comprised 180 trials, adhering to the same procedure as Experiment 1. The test session, also comprising 180 trials, presented only the numerical cue, requiring participants to recall memorized orientations from the training sessions without the grating presentation (Fig. 3*A*). This task required participants to rely entirely on internal representations developed through automaticity.

We first examined whether the main results from Experiment 1 could be replicated. Behaviorally, the four participants exhibited response errors of 4.90°, 3.78°, 7.35°, and 7.91° in the early stage, and 4.68°, 3.72°, 5.30°, and 8.65° in the late stage (Fig. 3*B*). Although three out of four participants showed reduced response errors in the late stage compared to the early stage, the differences did not reach statistical significance, $t < 1$. However, notably, in the early stage, the cued orientation was initially represented in the prefrontal cortex (364 to 676 ms) before being decoded from the hippocampus (800 to 1,076 ms; cluster-based permutation tests; $P < 0.05$, see Fig. 3*C*). This temporal hierarchy reversed in the late stage, with hippocampal representations preceding prefrontal ones (92 to 480 ms vs. 956 to 1,268 ms, respectively; cluster-based permutation tests; $P < 0.05$). This bidirectional temporal shift mirrors our core finding that increasingly rapid hippocampal decoding emerges as participants become more proficient at orientation reporting. Importantly, this pattern was observed across all participants (Fig. 3*C*), even for the one participant who did not exhibit a behavioral effect. Additionally, ripple rates in the hippocampus progressively increased during the immediate retrieval period as participants became more automatic in performing the task, $F(1,5) = 3.52$, $P = 0.026$, $\eta_p^2 = 0.54$, aligning with the observations from Experiment 1.

We further examined the data recorded across 9 training sessions. Behaviorally, the response errors for training sessions 1 to 9 were as follows: 9.93°, 5.39°, 5.84°, 6.56°, 5.39°, 5.01°, 4.31°, 6.63°, and 5.91° (Fig. 4 *A*, *Left* panel). Response times for the same sessions were 1,563 ms, 1,514 ms, 1,397 ms, 1,328 ms, 1,335 ms, 1,303 ms, 1,193 ms, 1,172 ms, and 992 ms, respectively (Fig. 4 *A*, *Right* panel). We conducted repeated-measures ANOVAs on response errors and response times, with the number of training sessions as a factor. Significant effects were observed for response errors, $F(1,8) = 4.48$, $P = 0.002$, $\eta_p^2 = 0.6$, and response times, $F(1,8) = 2.99$, $P = 0.018$, $\eta_p^2 = 0.5$. As illustrated in Fig. 4 *A*, *Left* panel, participants' response errors already reached a plateau after the first training session in this simple orientation recall task. This was confirmed by follow-up comparisons: Response errors in the first training session were significantly larger than those in sessions two, three, five, seven, and nine, all $ts > 3.3$, $ps < 0.046$. In contrast, response times showed a significant linear decrease over training sessions ($R^2 = 0.97$), with a positive slope significantly smaller than zero ($P < 0.001$). These findings suggest that while participants' accuracy stabilized early during training, their response speed continued to improve with extensive practice, indicating ongoing facilitation in task execution.

Notably, in the test session, response errors and response times were 6.30° and 984 ms, respectively, showing no significant differences from those in training session nine, both $ts < 1$. This finding suggests that, following extensive training, participants achieved automaticity in memory retrieval, enabling them to recall the cued orientation solely from internal memory representations.

To examine neural representations of cued orientation in the hippocampus and prefrontal cortex across different sessions, we performed comprehensive decoding analyses spanning training sessions two to nine and the test session. As shown in Fig. 4*B*, hippocampal decoding consistently emerged during early time windows following cue presentation. Specifically, significant decoding windows were observed at 268 to 540 ms, 316 to 700 ms, 152 to 560 ms, 160 to 524 ms, 344 to 676 ms, 404 to 564 ms, 180 to 460 ms, and 212 to 364 ms for training sessions two to nine, respectively, and at 4 to 356 ms for the test session (cluster-based permutation tests; $P < 0.05$). These results highlight stable early engagement of the hippocampus after training. Following the hippocampal representation of the cued orientation, decodable signals were detected in the prefrontal cortex, but only during training sessions two to seven, at 912 to 1,300 ms, 912 to 1,300 ms, 884 to 1,340 ms, 936 to1,208 ms, 960 to 1,160 ms, and 1,028 to 1,196 ms, respectively (cluster-based permutation tests; $P < 0.05$). This dissociation reflects a fundamental transition in memory systems as automaticity develops. Initially, task performance relies on both hippocampal processing and prefrontal cortex engagement. However, as skills consolidate and automaticity is achieved, the task becomes dependent solely on hippocampal processing, while prefrontal contributions diminish entirely. The persistent hippocampal decoding across all sessions underscores its continued role in automated memory retrieval, whereas the absence of prefrontal signatures in later sessions marks the cessation of its supervisory control after skill consolidation (27).

Notably, we also aimed to investigate what specific information was being decoded from neural activity. To this end, we attempted to decode the duration of the mouse response execution (i.e., the time taken to complete the mouse movement) to assess whether the hippocampus and other structures were encoding response-related processes. However, our analyses revealed that neural activity exclusively encoded the stimulus itself, rather than the response duration for each trial (*SI Appendix*, Fig. S5).

After prefrontal contributions diminished, we hypothesized that task performance in training sessions eight, nine, and the test session became solely dependent on hippocampal processing. Specifically, we predicted that hippocampal ripples—known to support memory retrieval processes (12, 14, 15)—would correlate with participants' behavioral performance, underscoring their central role in recall. To test this, we divided all trials into two groups: those with ripple occurrences and those without, and compared response times, which had significantly decreased over extensive practice. The results confirmed our hypothesis. In these later sessions, trials with hippocampal ripple occurrences exhibited significantly faster response times compared to those without (training session eight: mean reduction in RT = 37 ms, $t(3) = 5.67$, $p = 0.011$, Cohen's d = 2.83; training session nine: mean reduction in RT = 27 ms, $t(3) = 3.24$, $p = 0.048$, Cohen's d = 1.62; test session: mean reduction in RT = 72 ms, $t(3) = 8.07$, $p = 0.004$, Cohen's d = 4.03). Notably, this effect was absent during training sessions one through seven ($ts < 2.6$, $ps > 0.08$), suggesting that hippocampal ripples began mediating the speed of memory retrieval only after prefrontal contributions had ceased.

Downloaded from https://www.pnas.org by SOUTHERN MEDICAL UNIVERSITY on February 26, 2026 from IP address 58.249.1.69.

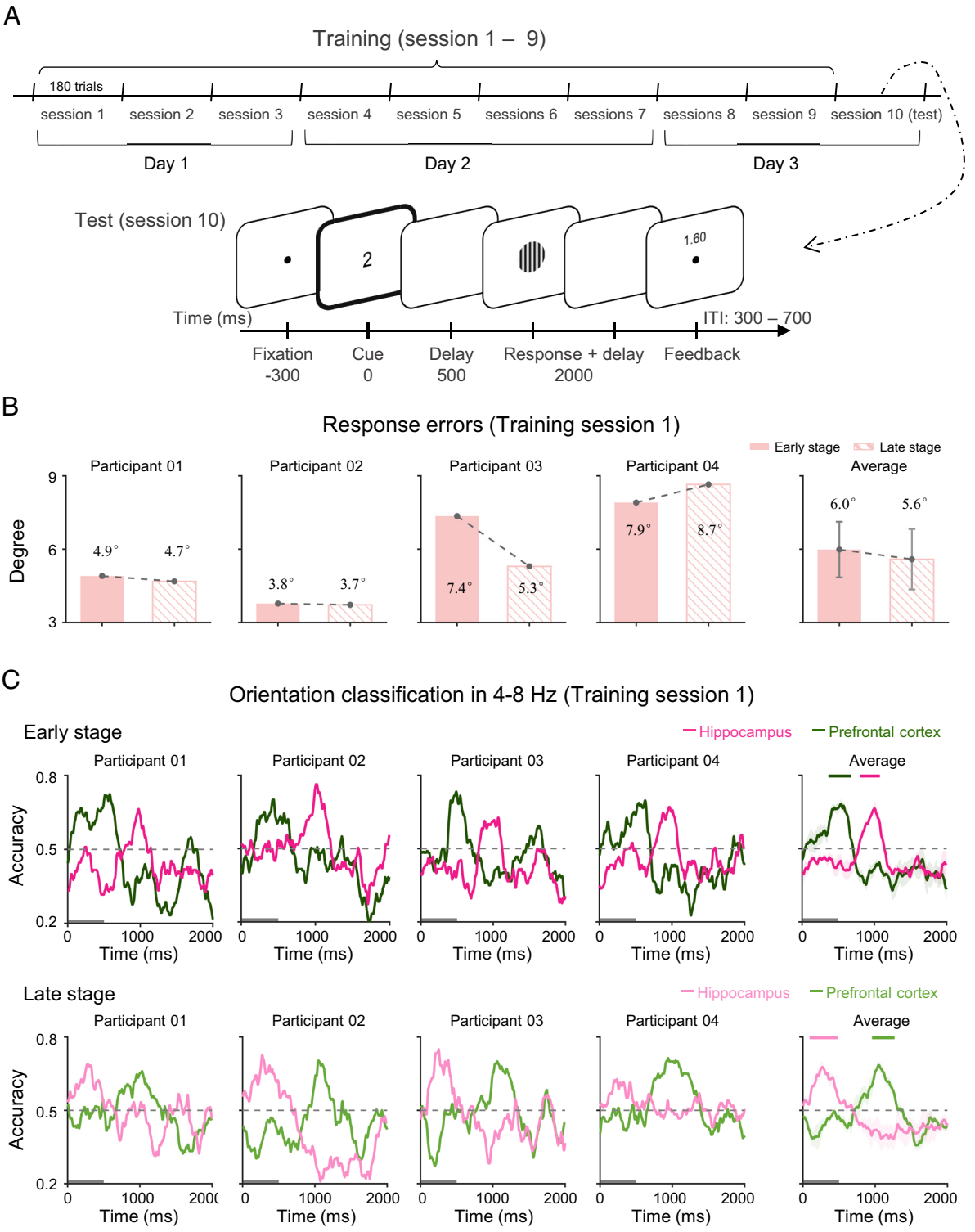


Fig. 3. (*A*) The procedure for Experiment 2. Over three consecutive days, participants completed nine training sessions and one test session. Each training session consisted of 180 trials, identical to the procedure used in Experiment 1, amounting to 1,620 trials in total. The *Bottom* panel illustrates the paradigm for the test session (180 trials), where only a cue was presented without the grating display, requiring participants to recall the memorized orientation from prior learning. (*B*) Mean response errors for individual participants during the early and late stages of the first training session, along with their averaged errors. Error bars represent ±1 SEM. (*C*) Decoding accuracies for the hippocampus and prefrontal cortex during the early (first 90 trials) and late (last 90 trials) stage of the first training session. Individual participant data and group averages are shown. Colored shaded areas around the lines represent ±1 SEM across all participants, and the horizontal bars indicate significant clusters following a cluster-based permutation test ($P < 0.05$). The gray segments on the X-axis denote the presentation of the cue.

Discussion

The findings from our experiments highlight the dynamic role of hippocampal ripples in retrieval during automaticity. In Experiment 1, after 180 trials of practice, ripple rates increased from the early to late stages, and were negatively correlated with the reduction in response errors across participants (n = 14). However, as data collection involved epilepsy patients in a unique clinical setting, the limited sample size necessitates caution when interpreting these correlation results. In Experiment 2, we further

Downloaded from https://www.pnas.org by SOUTHERN MEDICAL UNIVERSITY on February 26, 2026 from IP address 58.249.1.69.

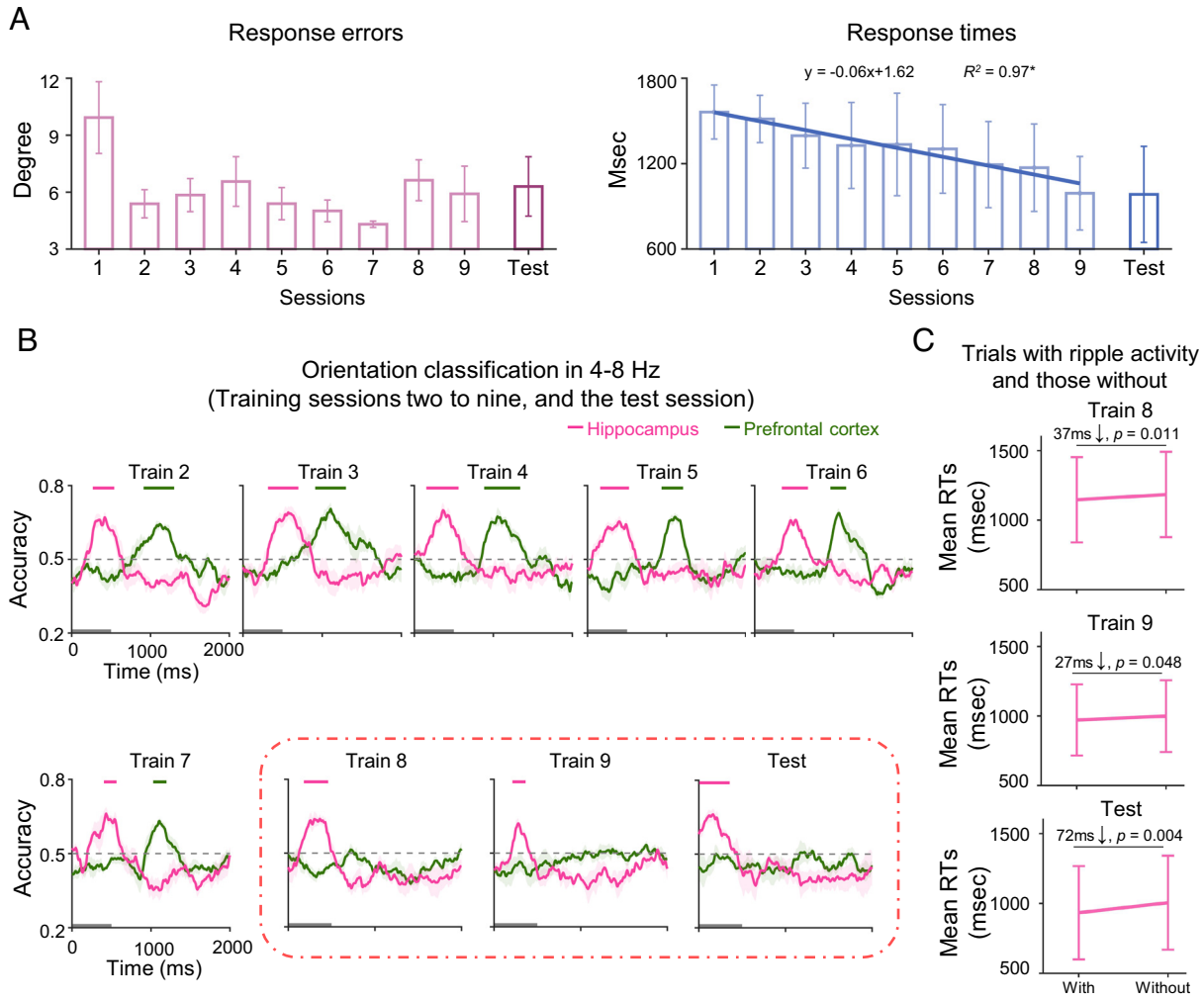


Fig. 4. (*A*) Behavioral performance, represented by response errors and response times, across the training and test sessions. Notably, response times followed a linear model (R^2 = 0.94; with a positive slope larger than zero, $P < 0.001$). (*B*) Decoding accuracies for the hippocampus and prefrontal cortex during training sessions two through nine, and the test session. Colored shaded areas around the lines represent ±1 SEM across all participants, and the horizontal bars indicate significant clusters following a cluster-based permutation test ($P < 0.05$). The gray segments on the X-axis denote the presentation of the cue. (*C*) Response times for two trial types—those accompanied by hippocampal ripple occurrences and those without—across training sessions eight and nine, as well as the test session. Error bars represent ±1 SEM.

demonstrated that as prefrontal contributions diminished, task performance in the later training sessions (eight, nine, and the test session) relied exclusively on hippocampal processing. Trials with hippocampal ripple occurrences exhibited significantly faster response times than those without. These findings suggest a shift in increased reliance on hippocampal ripples to support efficient memory retrieval following extensive practice, consistent with prior studies linking ripple activity to memory retrieval (e.g., 12, 34).

Notably, the methods used to detect ripples remain a topic of debate (35). While Liu et al. provide guidelines for distinguishing hippocampal sharp wave ripples from other fast oscillations, questions persist regarding the classification and functional roles of these activities. For instance, it has been proposed that multiple categories of high-frequency oscillations may exist and that hippocampal ripples could represent computations distinct from similar activity in other brain regions. This raises the need to clarify whether the observed ripple dynamics reflect a homogeneous or region-specific phenomenon. Future studies should consider alternative detection methods and incorporate region-specific analyses to better understand the role of ripples in learning and memory. Nevertheless, the ripple detection approach we employed aligns with widely used methods in prior human memory research (e.g., 12). Our results clearly demonstrate a temporal progression of ripple activity as learning advances, underscoring their critical role in memory retrieval during the transition to automaticity.

Automaticity is traditionally thought to involve regions such as the basal ganglia, which are associated with procedural memory (36–39), this does not entirely rule out the possibility that in healthy individuals, the hippocampus plays a role in the acquisition of automaticity, given its well-established link to long-term memory formation (40–42). It is possible that the earlier retrieval signals we observed in the hippocampus reflect interactions with basal ganglia circuits, even if we could not record these directly. Moreover, theories such as the competitive memory systems framework suggest a dynamic interplay between the hippocampus and basal ganglia, particularly during the transition from controlled to automatic processing (43). This emphasizes that hippocampal changes may occur in concert with changes elsewhere in the brain.

In our study, we demonstrate that during task learning information is available in the hippocampus about the to-be-reported stimulus earlier and earlier in time. This is a test of the predictions of theories of automaticity using the high temporal and

Downloaded from https://www.pnas.org by SOUTHERN MEDICAL UNIVERSITY on February 26, 2026 from IP address 58.249.1.69.

spatial resolution of human iEEG. Moving forward, future research should focus on investigating the specific mechanisms underlying the dynamic changes during automaticity in the hippocampus.

Methods

The present study was conducted according to the latest version of the Declaration of Helsinki and approved by the Medical Ethics Committee of Guangdong Sanjiu Brain Hospital (2023–02–006).

Participants. Eighteen patients (14 males and 4 females, ages 12 to 42 y) at Guangdong Sanjiu Brain Hospital participated in Experiment 1, and 4 patients (2 males and 2 females, ages 22 to 37 y) at Guangdong Sanjiu Brain Hospital and University of Hongkong Shenzhen Hospital participated in Experiment 2. All patients were implanted with clinical depth electrodes for diagnostic purposes only as part of their evaluation for neurosurgical epilepsy treatment. Each depth electrode (0.8 mm in diameter) had 8, 10, 12, 14, or 16 contacts that were 1.5 mm apart and 2 mm in contact length. All participants gave verbal or written informed consent to participate in research.

Paradigm and Design. In Experiment 1, each trial began when the participant initiated it by pressing the spacebar. Afterward, as illustrated in Fig. 1*A*, a fixation point was presented for 300 ms, followed by the first sine-waved grating (radius = 1.25 degree; frequency = 7 Hz) for another 300 ms. After the presentation of a mask (for 100 ms) and a delay (1,200 ms), the second grating was then presented for 300 ms, followed by another mask (100 ms) and delay (1,200 ms). Participants were asked to memorize the orientations of these two gratings. Subsequently, a numerical cue (presented for 500 ms) indicating which grating's orientation had to be reported, followed by a delay of 1,500 ms. A probe grating with an orientation of either 0 or 90° was presented until response, and participants were asked to utilize a mouse to rotate the test grating to the memorized orientation. If the response time was less than 3,000 ms, a blank display was presented for up to 3,000 ms. Feedback was provided, indicating the difference between the chosen and correct orientation. The experimental script for stimulus presentation and behavioral data collection was written in Psychtoolbox (44) on MATLAB (version 2021b; The MathWorks Inc., Natick, MA).

Notably, the two gratings were presented sequentially. The orientation of the first grating was selected from one of two ranges: 25 ± 10° (i.e., 15 to 35°) or 45 ± 10° (i.e., 35 to 55°). Similarly, the orientation of the second grating was chosen from 155 ± 10° (i.e., 145 to 165°) or 135 ± 10° (i.e., 125 to 145°). Orientation selection was counterbalanced across participants, and once assigned, the specific orientations remained fixed throughout the experiment. For example, if the third participant was assigned the orientations 27° and 153°, they encountered these stimuli in all trials. Response errors were calculated relative to these absolute values. Participants completed 10 practice trials followed by two learning stages, each consisting of 90 trials.

Experiment 2 comprised ten sessions conducted over three consecutive days, including nine training sessions and one test session. Each training session consisted of 180 trials, following the same procedure as in Experiment 1, resulting in a total of 1,620 trials across the training sessions. The test session also contained 180 trials; however, only the numerical cue was presented, requiring participants to recall the memorized orientations from the training sessions without the grating presentation (Fig. 3*A*).

Recordings and Preprocessing. The intracranial EEG (iEEG) recordings were acquired using a Nihon Kohden system at a sampling rate of 500, 1,000, or 2,000 Hz. A common contact, used as the reference for the online recording data, was placed subcutaneously and recorded simultaneously with the depth electrodes. The offline preprocessing was performed in MATLAB 2021b (MathWorks Inc), using EEGLAB (45), along with in-house MATLAB code. Contacts within each electrode that were deemed noisy or corrupted contacts upon visual inspection, were excluded from further analysis. Signals were rereferenced to the average activity across all contacts (46), and then resampled at 250 Hz. We removed 50 Hz power line noise prior to subsequent analyses using Hamming-windowed FIR filters (order of 180), and then high-pass filtered the data above 0.3 Hz using a second-order Butterworth filter. Continuous iEEG was segmented in epochs from −4,700 ms to 4,500 ms relative to the cue onset. Epochs were baseline-normalized by using the whole epoch as baseline to improve signal-to-noise ratio (47). For behavioral analysis, we calculated memory performance by taking the absolute value of the difference between the target value and the response value, referred to as response errors.

In Experiment 2, due to the limited number of patients included, we excluded trials where response times exceeded 10 s or where no mouse response was recorded. Subsequently, response times were log-transformed for analysis.

Removing Potential Contacts Contaminated By Epileptiform Activity. To identify trials in which transient epileptiform activity may be present, we examined iEEG recordings captured from electrodes. In previously published work, epileptiform artifacts were identified by looking for trials displaying excessive variance or kurtosis in the iEEG signal (14, 48). We calculated and sorted the mean iEEG voltage across all trials and divided the distribution into quartiles. We identified trial outliers by setting a threshold, $Q3+w*(Q3-Q1)$, where Q1 and Q3 are the mean voltage boundaries of the first and third quartiles, respectively. A team of epileptologists empirically determined the weight w to be 2.3. We excluded all trials with mean voltage that exceeded this threshold. The average percent removed across all sessions in each participant due to either system-level noise or transient epileptiform activity was 1.4 ± 3.26% of all electrodes and 0.93 ± 1.68% of all trials in Experiment 1, and 3.24 ± 1.53% of all electrodes and 5.72 ± 4.31% of all trials in Experiment 2.

Contact Reconstruction and Localization. We collected 2301 depth recording contacts (127.8 ± 35.2 per subject) and 702 depth recording contacts (175.5 ± 31.2 per subject) in Experiments 1 and 2, respectively. To localize their precise positions in the brain, we first registered postoperative computed tomography (CT) images to preoperative T1-weighted MR images using FreeSurfer v6.0.0 (49), following the iElvis pipeline (50). We inspected the quality of the registration and manually labeled each contact location on the T1-registered CT images, which were then mapped onto a standard MNI space (Fig. 1*C*). To further determine the exact contact locations belonging to different brain regions, we assigned contact MNI coordinates to each brain region according to FreeSurfer's automatic parcellation. We went through each contact and assigned the closest cortical/subcortical label for each region of interest (ROI), i.e., hippocampus (70 and 48 contacts in Experiments 1 and 2, respectively), middle-temporal gyrus (273 contacts in Experiment 1), and prefrontal cortex (196 and 149 contacts in Experiments 1 and 2, respectively).

Time Frequency Analysis. To extract the power for the whole frequency bands (ranging from 1 to 120 Hz), preprocessed iEEG epochs (−4,700 ms to 4,500 ms relative to the cue onset) were convolved with a set of Morlet wavelets. The number of cycles of each wavelet was logarithmically spaced between 4 and 20 to strike a good balance between temporal and frequency precision. We used 1 or 5 Hz as a step to obtain frequency power for low (1 to 30 Hz) or high (35 to 120 Hz) frequencies, respectively. The power values within our focused epochs (−3,700 ms to 2,000 ms relative to the cue onset; avoiding edge artifacts from wavelet convolution) were z-scored by subtracting the average value and dividing by the SD across all epochs (trials). To accurately compare power between learning stages, we subtracted the mean power from −500 ms to −300 ms prior to the first grating stimulus for each stage.

Decoding Cued Orientation. We employed a Support Vector Machine (SVM) approach to create two classifiers aimed at distinguishing between two distinct orientations over time following the presentation of the cue. The error-correcting output codes (ECOC) were used to decode the orientation information, effectively addressing multiclass categorization problems by aggregating results from multiple binary classifiers. The ECOC model was implemented through the 'fitcecoc()' function in MATLAB. For each orientation, separate trials were selected for training and testing. Specifically, the SVM decoding at each time point involved a threefold cross-validation procedure, where data from 2/3 of the trials (selected randomly) were used to train the classifier. Subsequently, the performance of the classifier was evaluated using data from the remaining 1/3 of trials. To mitigate any potential biases associated with trial assignment to groups, we iterated the entire procedure 10 times, each with new random assignments of trials to the three groups (for more details, see ref. 51). This SVM decoding analysis was conducted separately for different learning stages and frequency bands.

Downloaded from https://www.pnas.org by SOUTHERN MEDICAL UNIVERSITY on February 26, 2026 from IP address 58.249.1.69.

To assess decoding accuracy against chance level (50%) at each time point while controlling for multiple comparisons, we used a cluster-based permutation test against a null-distribution shuffled from 1,000 iterations using a Monte Carlo randomization procedure. Specifically, a one-tailed *t* test was performed against 0.5 to identify above-chance accuracy, and time windows with t-values larger than a threshold (at $P = 0.05$) were combined into contiguous clusters based on adjacency. The cluster statistics were calculated as the sum of the t values within each cluster. To create a null distribution of clusters, the SVM procedure was iterated 1,000 times, with the orientation labels randomized and assigned to each trial to ensure independence from observed responses. The largest clusters for random orientation labels were identified per iteration, forming the null distribution of clusters. Clusters were determined to be significant if their cluster statistics exceeded the 95th percentile of the null distribution.

We also analyzed other frequency bands, including the delta (1 to 3 Hz), alpha (8 to 12 Hz), beta (13 to 30 Hz), slow (35 to 60 Hz), and fast gamma bands (60 to 120 Hz). In those frequency bands we were unable to obtain robust decoding in the hippocampus, middle-temporal gyrus, and prefrontal cortex (*SI Appendix*, Fig. S4).

Ripple Activity. In addition to system-level line noise, eye-blink artifacts, sharp transients, and interictal epileptiform discharges (IEDs) may erroneously be identified as ripples after high-pass filtering. To mitigate this issue, we implemented a previously reported automated trial-level artifact rejection method (13). This involved calculating a z-score for each time point based on both the gradient (first derivative) and amplitude after applying a 250 Hz high-pass filter (primarily for epileptogenic spike identification). Any time point exceeding a z-score of 5 for either gradient or high frequency amplitude was flagged as artifact, with an additional 100 ms time window before and after each identified time point also classified as artifact.

To detect ripple activities, we initially bandpass filtered the iEEG signals (resampled at 1,000 Hz to accommodate the high frequency ripples, except for one participant whose raw signal was sampled at 500 Hz and was not resampled) within the predefined ripple band (70 to 180 Hz; see ref. 12 using a twenty-order finite filter. Subsequently, we extracted the instantaneous voltage within this ripple band for each trial. We selected time points where the voltage exceeded or fell below 2.5 SDs from the mean voltage of the filtered trials. Only events (successive time points) that were at least 25 ms in duration and exhibited a maximum voltage exceeding or a minimum voltage dropping below 3 SDs were retained as ripples for further analysis, in line with procedures employed in previous studies (14, 52). Adjacent ripples separated by less than 15 ms were combined (53). We identified each ripple meeting these criteria and assigned each identified ripple a start time index and an end time index. The duration of each ripple was defined as the difference between these indices. We only considered ripples whose median duration fell within the significant clusters obtained from the SVM decoding results and computed the ripple rates (i.e., the frequency of ripple activities per second) during this period. This ensured a fair comparison between different clusters, considering their varying lengths in time.

Data, Materials, and Software Availability. Code and behavioral data have been deposited in Github (https://github.com/Zoeezhang/Automaticity-speeds-the-retrieval-of-instances-from-the-human-hippocampus) (54). We have agreed that anonymized intracranial EEG data supporting the findings of this study will also be made available. All of these data will be uploaded to GitHub.

ACKNOWLEDGMENTS. This research was supported by the National Science and Technology Innovation 2030 Major Program (2022ZD0204802), the National Social Science Foundation of China (20&ZD296), the Ministry of Education Project of Key Research Institute of Humanities and Social Sciences in Universities (22JJD190006) and the Natural Science Foundation of Guangdong grant (2023A1515012789) to BW; the Wellcome Trust Discovery Award (227420) and the National Institute for Health and Care Research Oxford Health Biomedical Research Centre (203316) to OJ.

Author affiliations: [a]Center for Studies of Psychological Application, South China Normal University, Guangzhou 510631, China; [b]Institute for Brain Research and Rehabilitation, South China Normal University, Guangzhou 510631, China; [c]Department of Experimental and Applied Psychology, Vrije Universiteit Amsterdam, Amsterdam 1081HV, The Netherlands; [d]Department of Neurosurgery, Guangdong Sanjiu Brain Hospital, Guangzhou 510515, China; [e]Department of Psychology, Vanderbilt University, Nashville, TN 37235; [f]Center for Integrative and Cognitive Neuroscience, Vanderbilt University, Nashville, TN 37235; [g]Department of Neurosurgery, The University of Hong Kong Shenzhen Hospital, Shenzhen 518053, China; and [h]Department of Psychiatry and Experimental Psychology, University of Oxford, Oxford OX13BN, United Kingdom

1. G. D. Logan, Toward an instance theory of automatization. *Psychol. Rev.* **95**, 492–527 (1988).
2. G. F. Woodman, N. B. Carlisle, R. M. G. Reinhart, Where do we store the memory representations that guide attention? *J. Vis.* **13**, 1–17 (2013).
3. N. B. Carlisle, J. T. Arita, D. Pardo, G. F. Woodman, Attentional templates in visual working memory. *J. Neurosci.* **31**, 9315–9322 (2011).
4. R. J. Addante, A. J. Watrous, A. P. Yonelinas, A. D. Ekstrom, C. Ranganath, Prestimulus theta activity predicts correct source memory retrieval. *Proc. Natl. Acad. Sci. U.S.A.* **108**, 10702–10707 (2011).
5. A. R. Backus, J. M. Schoffelen, S. Szebényi, S. Hanslmayr, C. F. Doeller, Hippocampal-prefrontal theta oscillations support memory integration. *Curr. Biol.* **26**, 450–457 (2016).
6. J. Fell *et al.*, Medial temporal theta/alpha power enhancement precedes successful memory encoding: Evidence based on intracranial EEG. *J. Neurosci.* **31**, 5392–5397 (2011).
7. M. C. Fellner *et al.*, Spectral fingerprints or spectral tilt? Evidence for distinct oscillatory signatures of memory formation. *PLoS Biol.* **17**, 1–30 (2019).
8. L. L. Colgin, Rhythms of the hippocampal network. *Nat. Rev. Neurosci.* **17**, 239–249 (2016).
9. M. E. Hasselmo, What is the function of hippocampal theta rhythm?–Linking behavioral data to phasic properties of field potential and unit recording data. *Hippocampus* **15**, 936–949 (2005).
10. N. A. Herweg, E. A. Solomon, M. J. Kahana, Theta oscillations in human memory. *Trends Cogn. Sci.* **24**, 208–227 (2020).
11. N. Axmacher, C. E. Elger, J. Fell, Ripples in the medial temporal lobe are relevant for human memory consolidation. *Brain* **131**, 1806–1817 (2008).
12. Y. Norman *et al.*, Hippocampal sharp-wave ripples linked to visual episodic recollection in humans. *Science* **365**, eaax1030 (2019).
13. B. P. Staresina *et al.*, Hierarchical nesting of slow oscillations, spindles and ripples in the human hippocampus during sleep. *Nat. Neurosci.* **18**, 1679–1686 (2015).
14. A. P. Vaz, S. K. Inati, N. Brunel, K. A. Zaghloul, Coupled ripple oscillations between the medial temporal lobe and neocortex retrieve human memory. *Science* **363**, 975–978 (2019).
15. A. P. Vaz, J. H. Wittig, S. K. Inati, K. A. Zaghloul, Replay of cortical spiking sequences during human memory retrieval. *Science* **367**, 1131–1134 (2020).
16. A. Ylinen *et al.*, Sharp wave-associated high-frequency oscillation (200 Hz) in the intact hippocampus: Network and intracellular mechanisms. *J. Neurosci.* **15**, 30–46 (1995).
17. J. E. Kragel, J. L. Voss, Looking for the neural basis of memory. *Trends Cogn. Sci.* **26**, 53–65 (2022).
18. Z. Bahmani, M. R. Daliri, Y. Merrikhi, K. Clark, B. Noudoost, Working memory enhances cortical representations via spatially specific coordination of spike times. *Neuron* **97**, 967–979.e6 (2018).
19. E. F. Ester, T. C. Sprague, J. T. Serences, Parietal and frontal cortex encode stimulus-specific mnemonic representations during visual working memory. *Neuron* **87**, 893–905 (2015).
20. S. M. Ravizza, M. R. Delgado, J. M. Chein, J. T. Becker, J. A. Fiez, Functional dissociations within the inferior parietal cortex in verbal working memory. *Neuroimage* **22**, 562–573 (2004).
21. G. D. Logan, Repetition priming and automaticity: Common underlying mechanisms? *Cogn. Psychol.* **22**, 1–35 (1990).
22. R. M. Shiffrin, W. Schneider, Controlled and automatic human information processing: II. Perceptual learning, automatic attending and a general theory. *Psychol. Rev.* **84**, 127 (1977).
23. F. Verbruggen, G. D. Logan, Response inhibition in the stop-signal paradigm. *Trends Cogn. Sci.* **12**, 418–424 (2008).
24. G. D. Logan, An instance theory of attention and memory. *Psychol. Rev.* **109**, 376–400 (2002).
25. G. D. Logan, W. B. Cowan, On the ability to inhibit thought and action: A theory of an act of control. *Psychol. Rev.* **91**, 295 (1984).
26. W. Schneider, J. M. Chein, Controlled & automatic processing: Behavior, theory, and biological mechanisms. *Cogn. Sci.* **27**, 525–559 (2003).
27. M. W. Cole, W. Schneider, The cognitive control network: Integrated cortical regions with dissociable functions. *Neuroimage* **37**, 343–360 (2007).
28. J. R. Anderson, *Cognitive Psychology and Its Implications* (Macmillan, 2005).
29. T. K. Leonard, K. L. Hoffman, Sharp-wave ripples in primates are enhanced near remembered visual objects. *Curr. Biol.* **27**, 257–262 (2017).
30. T. Schreiner *et al.*, Spindle-locked ripples mediate memory reactivation during human NREM sleep. *Nat. Commun.* **15**, 5249 (2024).
31. C. Kerrén, S. Michelmann, C. F. Doeller, Hippocampal ripples initiate cortical dimensionality affiliations. bioXriv [Preprint] (2025), https://doi.org/10.1101/2025.04.22.649929 (Accessed 28 April 2025).
32. N. M. Hill, W. Schneider, "Brain changes in the development of expertise: Neuroanatomical and neurophysiological evidence about skill-based adaptations" in *The Cambridge Handbook of Expertise and Expert Performance* (2012), pp. 653–682, 10.1017/cbo9780511816796.037.
33. J. M. Chein, W. Schneider, The brain's learning and control architecture. *Curr. Dir. Psychol. Sci.* **21**, 78–84 (2012).
34. S. P. Jadhav, C. Kemere, P. W. German, L. M. Frank, Awake hippocampal sharp-wave ripples support spatial memory. *Science* **336**, 1454–1458 (2012).
35. A. A. Liu *et al.*, A consensus statement on detection of hippocampal sharp wave ripples and differentiation from other fast oscillations. *Nat. Commun.* **13**, 6000 (2022).
36. R. A. Poldrack *et al.*, The neural correlates of motor skill automaticity. *J. Neurosci.* **25**, 5356–5364 (2005).
37. H. H. Yin, B. J. Knowlton, The role of the basal ganglia in habit formation. *Nat. Rev. Neurosci.* **7**, 464–476 (2006).
38. F. G. Ashby, B. O. Turner, J. C. Horvitz, Cortical and basal ganglia contributions to habit learning and automaticity. *Trends Cogn. Sci.* **14**, 208–215 (2010).
39. J. G. Waldschmidt, F. G. Ashby, Cortical and striatal contributions to automaticity in information-integration categorization. *Neuroimage* **56**, 1791–1802 (2011).
40. R. E. Clark, S. M. Zola, L. R. Squire, Impaired recognition memory rats after damage to the hippocampus. *J. Neurosci.* **20**, 8853–8860 (2000).
41. W. B. Scoville, B. Milner, Loss of recent memory after bilateral hippocampal lesions. *J. Neurol. Neurosurg. Psychiatry* **20**, 11 (1957).

Downloaded from https://www.pnas.org by SOUTHERN MEDICAL UNIVERSITY on February 26, 2026 from IP address 58.249.1.69.

42. S. M. Zola *et al.*, Impaired recognition memory in monkeys after damage limited to the hippocampal region. *J. Neurosci.* **20**, 451–463 (2000).
43. R. A. Poldrack, M. G. Packard, Competition among multiple memory systems: Converging evidence from animal and human brain studies. *Neuropsychologia* **41**, 245–251 (2003).
44. D. H. Brainard, S. Vision, The psychophysics toolbox. *Spat. Vis.* **10**, 433–436 (1997).
45. A. Delorme, S. Makeig, EEGLAB: An open source toolbox for analysis of single-trial EEG dynamics including independent component analysis. *J. Neurosci. Methods* **134**, 9–21 (2004).
46. R. Lin *et al.*, Neural evidence for attentional capture by salient distractors. *Nat. Hum. Behav.* **8**, 932–944 (2024).
47. D. M. Groppe, S. Makeig, M. Kutas, Identifying reliable independent components via split-half comparisons. *Neuroimage* **45**, 1199–1211 (2009).
48. A. I. Jang, J. H. Wittig, S. K. Inati, K. A. Zaghloul, Human cortical neurons in the anterior temporal lobe reinstate spiking activity during verbal memory metrieval. *Curr. Biol.* **27**, 1700–1705 (2017).
49. B. Fischl, FreeSurfer. *Neuroimage* **62**, 774–781 (2012).
50. D. M. Groppe *et al.*, iELVis: An open source MATLAB toolbox for localizing and visualizing human intracranial electrode data. *J. Neurosci. Methods* **281**, 40–48 (2017).
51. G. Y. Bae, S. J. Luck, Dissociable decoding of spatial attention and working memory from EEG oscillations and sustained potentials. *J. Neurosci.* **38**, 409–422 (2018).
52. D. Khodagholy, J. N. Gelinas, G. Buzsáki, Learning-enhanced coupling between ripple oscillations in association cortices and hippocampus. *Science* **1979**, 369–372 (2017).
53. L. Roux, B. Hu, R. Eichler, E. Stark, G. Buzsáki, Sharp wave ripples during learning stabilize the hippocampal spatial map. *Nat. Neurosci.* **20**, 845–853 (2017).
54. Y. Zhang *et al.*, Data from "Automaticity-speeds-the-retrieval-of-instances-from-the-human-hippocampus". GitHub. https://github.com/Zoeezhang/Automaticity-speeds-the-retrieval-of-instances-from-the-human-hippocampus. Deposited 5 October 2025.

Downloaded from https://www.pnas.org by SOUTHERN MEDICAL UNIVERSITY on February 26, 2026 from IP address 58.249.1.69.